ISSN 2738-9898 (Print) ISSN 2738-9901 (Online)

A study of Urban Heat Island relating "Local Climate Zones" using Landsat Images- The Case of Kathmandu Valley

Deepak Bikram Thapa Chettri[1], Kusum Deo[1] and Pukar Regmi[1]

[1] Department of Civil Engineering, Kantipur City College, Kathmandu, Nepal

E-mail: *deepakthapa@kcc.edu.np, kusumdeo@kcc.edu.np, pukarregmi@kcc.edu.np*

Received on: 21st, Oct., 2022

Accepted for publication: 1st, Dec., 2022

Abstract

Local Climate Zone (LCZ) classification has been intensively used in classification of urban and rural landscapes in the cities, which includes urban temperature studies. The urban heat island (UHI) in Kathmandu valley (Kathmandu, Bhaktapur, and Lalitpur), has been analyzed and standardized, which mainly focused on the Local Climate Zones (LCZs). The LCZs has distribute the landscape into homogeneous types on the basis of structural type, land surface cover, materials used, and into the anthropogenic activities. Such standardized classification has improved the meaning of urban research and made it easier to compare results among cities around the world. Landsat images, Google Earth, and SAGA-GIS software were used for creating LCZ map for Kathmandu for both March 2013 and March 2019 Landsat 8 TM/ETM+/OLI imagery was used to estimate land surface temperature (LST) For the estimation of LST world urban database and access portal tools (WUDAPT) algorithm was used considering emissivity. The result thus shows that the difference within the built-up scheme is around 2-4 °C whereas the difference between Building and Land cover types on the comparison is around 5-10°C. The disparity in building the land cover types shows that the UHI impact is present in the Kathmandu valley.

Keywords: Local Climate Zones (LCZ), Land Surface Temperature (LST), Landsat Image, Urban Heat Island.

1. Introduction:

Urban expansion is occurring at an unprecedented rate, leading it to a drastic change in. According to the UN demographic statistics, more than 54% of the world's population now live in urban areas, and this number will reach 66% by 2050[1]. Roads, buildings, parks, and gardens are being built to replace the natural cover of neighborhood forests, grasslands, and deserts. Such as Temperature, precipitation, humidity, winds, are affected to a lesser extent, cloud and radiation are all affected by land cover changes in cities. Also, this change has environmental implications, which often gets subtle in primitive area and it has sparsely populated the settlements, but in modern cities, the implications are long term [2].

Kathmandu, the capital city of Nepal, is part of a cosmopolitan and expansive valley that includes Lalitpur and Bhaktapur, Kathmandu. The Kathmandu Valley (KV) has synopsize such rapid growth of urban area. Therefore there is a transition. The transition of agriculturally productive peri-urban areas to rapid home development, which has expanded its outskirts in

a concentric zone way is occurring briskly. The urban built-up area has been expanding rapidly replacing those agricultural lands. Rapid urban expansion in corporation with unmanaged settlement and haphazard development has led to numerous socio-environmental challenges. Ineffective and inefficient land use, zoning, and land subdivision policies are at the core cause of these unmanaged developments in the KV[3].

Urban heat island (UHI) effect is one of the ecological consequences of urbanization [4]. "Urban Heat Island, refers to the atmospheric warmth of a city compared to its countryside". Urban heat island intensity (UHI) is an important metric used in measuring UHI effect. In spite of number of previous UHI/UDI studies [5, 6, 7, 8], the study has lacked a proper standard to categorize urban and rural areas. Hence, this has created variation in the results and it is difficult to compare the individual urban/rural related studies from one city to another. To deal with such kind of problem Steward and Oke proposed a classification scheme – "Local Climate Zones" [9] which has introduced a pedagogical and relevant solution which involves dividing various microclimatic environments into a particular zone known as Local Climate Zone (LCZ). The LCZ is mainly divided into built types and land cover types. Built types are further divided into zones based on fabric coverage and metabolism. Likewise, land cover types are further divided into seven zones as shown in Table 1.

Table 1: LCZ divided into built types and land cover types

LCZ	Building Types	LCZ	Land Cover Types
1	Compact high-rise	A	Dense trees
2	Compact midrise	B	Scattered trees
3	Compact low-rise	C	Bush, Scrub
4	Open high-rise	D	Low plants
5	Open midrise	E	Bare rock/paved
6	Open low-rise	F	Bare soil/sand
7	Lightweight low-rise	G	Water
8	Large Low-rise		
9	Sparsely built		
10	Heavy Industry		

Land Surface Temperature (LST) is being used in a variety of areas such as evapotranspiration, climate change, hydrological cycle, vegetation monitoring, urban climate, and environmental studies, among others [10, 11, 12, 13, 14. 15, 16, 17, 18]. Satellite-based thermal infrared (TIR) data purposefully linked to the LST through the radiative transfer equation. The retrieval of the LST from remotely sensed thermal infrared (TIR) data has grabbed much attention, especially from Landsat-8 TIR bands. Besides radiometric calibration and cloud screening, the determination of LSTs from space-based TIR measurements requires atmospheric corrections [19]. In the past, many studies have been put through to estimate LST from satellite-derived TIR data, by using different approaches and methods i.e. mono-window algorithm [20] and single-channel algorithm [21]. Before the invention of earth observation satellites (EOS), it was hard to estimate the LST of an area. But today, remotely sensed data is being used for LST estimation using thermal data.

2. Materials and Method:

2.1. Study Area:

The Kathmandu Valley comprising an area of approximately 664 km² is the administrative center of Nepal and home to the capital city, Kathmandu (1311 m above sea level). The Kathmandu Valley is located in the central-east part of Nepal and lies between latitudes 27°32'13'' and 27°49'10'' north and longitudes 85°11'31'' and 85°31'38'' east [22]. The Kathmandu valley ranges from 1144 m and is surrounded by the hills of the Mahabharata range up to 2717 m which form a bowl-shaped valley floor [23]. The Kathmandu Valley consists of numerous municipalities. Some of the areas on the outskirt are predominantly located in rural areas while some municipalities are located in the central urbanized areas. However, due to rapid urbanization, many of these rural village development committees are now characterized by urban expansion [22]. The climate here is sub-tropical cool temperate. Generally, the annual maximum and minimum air temperatures were between 29.7 °C in May and 2 °C in January, respectively. The heavy concentration of precipitation occurs from June to August as a

result of southeast monsoon winds [24].The study area of is shown in Fig.1

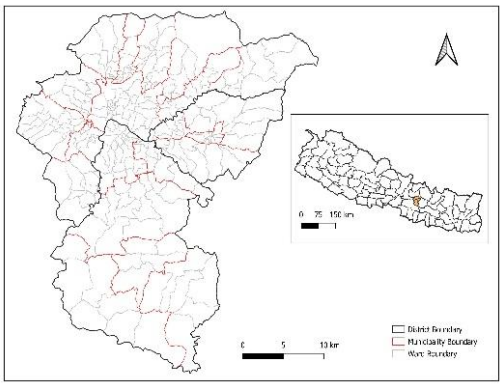

Figure 1: Study Area: Kathmandu Valley

2.2. Aim of Paper:

The aim of this paper is to determine the relationship between LST and LCZ classes with the Kathmandu Valley selected as a case study. Landsat 8 images (2019 and 2013) of Kathmandu valley were used to investigate LST, which were subsequently classified to show the surface UHI intensity. An improvised method of the World Urban Database and Portal Tool (WUDAPT) was also practiced to develop the LCZ map. Air temperature data was not used to test against the LST pattern of LCZ classes. LST of different LCZ classes characterized in an effort to inform urban climate researchers and urban planners about the influence of LCZ on local climate, leading to more sustainable urban planning in the valley.

2.3. Landsat 8 Data:

For the study of Local Climate Zoning and Land Surface Temperature Landsat 8 satellite images, Operational Land Imagery (OLI) and Thermal Infrared Sensor (TIRS) 15- to 30- meter multispectral data from Landsat 8 C1 Level- 1, were downloaded from United States Geological Survey (USGS). Thermal band (Band 10) was allocated (because Band 10 has wavelength of 10.6 to 11.9 micrometers with resolution of 100 meters) as the atmospheric brightness temperature in Kelvin (K), and the multispectral bands of Landsat-8 OLI were provided as surface reflectance. The satellite imageries were chosen such that the cloud coverage is less than 10%.

Table 2: Landsat TM/ETM+/OLI imagery used in this study a) LST calculation b) LCZ reconstruction, Kathmandu UTC + 5.45 hours

Landsat-ID	Acquisition date (YY-MM-DD)	Acquisition time UTC (Kath. valley)	Spatial resolution of TIR band (m)
LC8141041 2013085LGN02	2013-03-26	04:48:43	100
LC8141041 2019083LGN00	2019-03-24	04:47:55	100

2.4. LCZ mapping of the study area:

Several LCZ mapping schemes are available so far. For example, [25] follows a manual sampling of individual grid cells using Geo-Wiki, digitization of homogeneous LCZs, and a GIS-based approach using building data. [26, 27] follow object-based image analysis. [28, 29] follow supervised pixel-based classification.

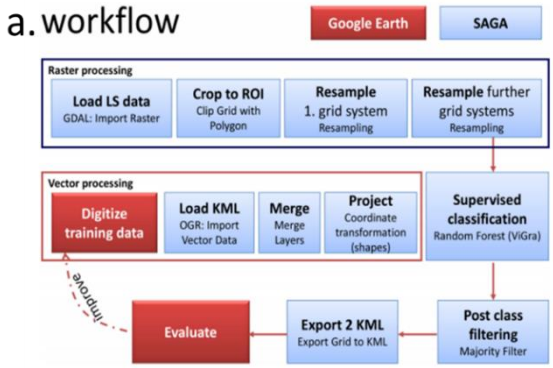

Figure 2: Overview of mapping process: work flow

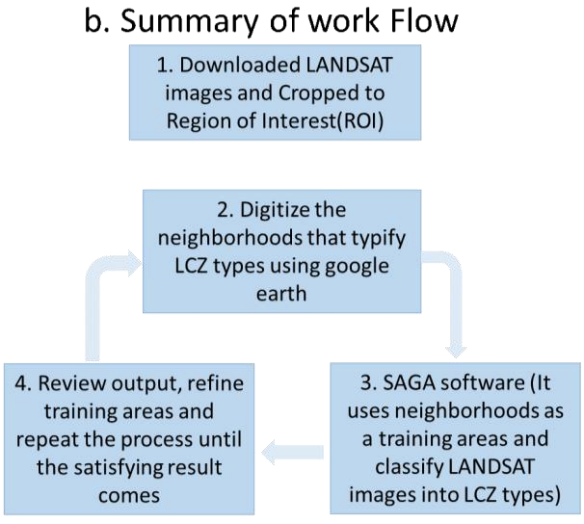

Figure 3: Summary of Work flow

In this study, the methodology provided by the World Urban Database and Access Portal Tools (http://www.wudapt.org/) has been adapted. WUDAPT has developed a basic process that makes the operation universal, with minimum data requirements, comparable between cities and operators, computationally and financially affordable, and simple to implement. Important aspects, preparation, and tools of the implemented workflow are shown in [Fig. 2(a)].

In this mapping process, Google Earth is used along with the high-resolution imagery of cities for identifying the appropriate training sites. The Landsat data which is used in this study for the classification can easily be acquired from the U.S. Geological Survey Earth explorer interface [Fig. 3]. For the geometrical preprocessing and the classification of the map, System for Automated Geoscientific Analysis (SAGA) is used as a platform. First, the downloaded Landsat is cropped to the region of interest (ROI). The training areas are digitized using Google Earth and loaded to SAGA in KML (Keyhole Markup Language) format. KML is a file format is usually used to display geographic data in an Earth browser such as Google Earth. In SAGA, the layers are merged and coordinates are transformed.

To obtain the LCZ map, sampling is followed by resampling, and post classifications are used. For verification, the produced LCZ map is checked on the Google Earth platform. If necessary, corrections are addressed by adding training areas, and the procedure is repeated to build the representative LCZ map.

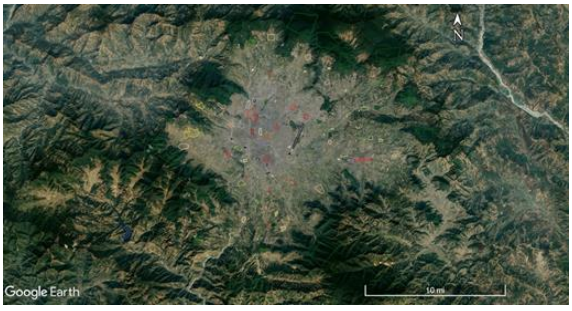

Figure 4: Training areas to develop LCZ map using (WUDAPT) algorithm

2.5. LST of the study area:

The methodology adopted by [31] as shown in Fig. 5 was used for the analysis purpose. Band operations are performed to apply the algorithm as mentioned in WUDAPT to calculate LST [32].

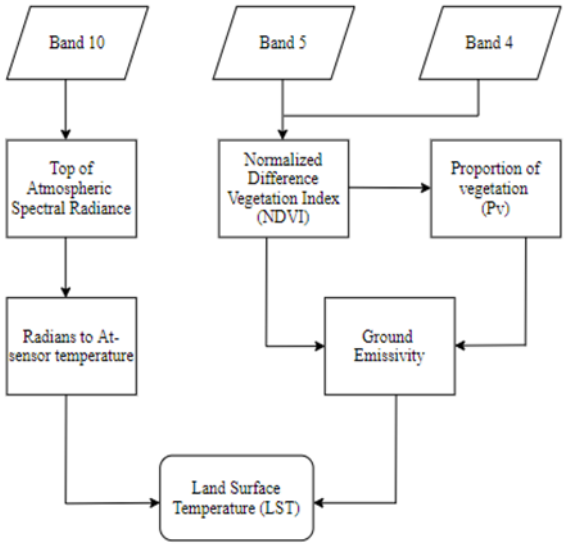

Figure 5: Flowchart of the Land Surface Temperature algorithm

Any object possessing a temperature above absolute zero Kelvin emits thermal infrared radiation. The signals received by radiometers on satellite can be converted to at-satellite radiance (L sensors using Eq. 1:

$$L\ Sensors = gain \times DN + bais \quad (1)$$

where L sensors is the spectral radiance of thermal band in W/(m^2 ster. mm); gain is the slope of the radiance conversion function; bias is the intercept of the radiance conversion function [33].

The gain and bias values are found in the metadata file provided with the satellite data.

Radiance values from the thermal band can then be transformed to at satellite brightness temperature using the thermal calibration constant given in the metadata file.

$$T\ sensor\ (TB) = [k2/(\ln\left(\frac{k1}{L\ sensor} + 1\right)] - 273.15 \quad (2)$$

where *T*' sensor is at satellite brightness temperature in degree Celsius; *K1* and *K2* are thermal calibration constants.

To relate the at-satellite brightness temperature and LST, the emissivity properties of an object plays an important role. The estimation of LST considering emissivity can be simplified using following the algorithm [32].

$$T = \frac{TB}{[1+ (\lambda \text{ x } TB / C2) \text{ x } \ln (e)]} \quad (3)$$

where, λ= wavelength of emitted radiance (λ=11.5 µm); *C2* = (h×c/s) =1.4388 x 10^{-2} m K = 14388 µm K; *h* = Planck's constant = 6.626 x10^{-34} J s; *s* = Boltzmann constant = 1.38 x10^{-23} J/K; *c* = velocity of light = 2.998 x 10^{8} m/s; *e* = emissivity

In the above Eq. 3, emissivity is an unknown value. There are various methods to predict the emissivity value from the satellite data. A method based on LULC classified map is the simplest one but the accuracy of LULC classification has a significant influence on emissivity prediction. Also, these methods use ratio values of vegetation and bare land.

One of the easier methods to predict emissivity is using NDVI image as given by [34]

$$e = 0.004\, Pv + 0.986 \quad (4)$$

where Pv is the proportion of vegetation obtained [35]

$$Pv = \left(\frac{NDVI - NDVImin}{NDVImax - NDVI\ min}\right)^2 \quad (5)$$

Where NDVI is a normalized difference vegetation index that is used to evaluate the content of vegetation present in an area.

3. Result and discussion:

LCZ and LST retrieval process is completed using WUDAPT algorithms [28] respectively. LCZ and LST maps are generated for Kathmandu Valley as shown in Fig. 6, for the years 2013 and 2019 respectively. Since the original LST calculation was in Kelvin but the degree Celsius (°C) is used as the basic unit for temperature in all analyses. As a result, the Kelvin to °C conversion is used, and the results are given in degrees Celsius.

3.1. Local climate zones:

First of all, three LCZ classes are absent in the urban areas: LCZ 1 (compact high-rise); LCZ 4 (open high-rise), and LCZ 5 (Open mid-rise). In the case of two cities i.e. Bhaktapur and Lalitpur, the administrative border indicated with a black line is connected with the capital city Kathmandu Fig. 1. In comparison to these cities, Kathmandu seems to have the highest settlement, Lalitpur is second and Bhaktapur has the least settlement. Bhaktapur is also the smallest district in Nepal. The core city of Bhaktapur in 2019 seems to have grown compared to 2013[37]. The settlement at Kathmandu has increased northward. The settlement is mostly LCZ 3 (Compact low-rise). All the cities (Kathmandu, Bhaktapur, and Lalitpur) are very old historic cities and the settlement pattern is mostly compact. Each house is joined with the adjacent buildings.

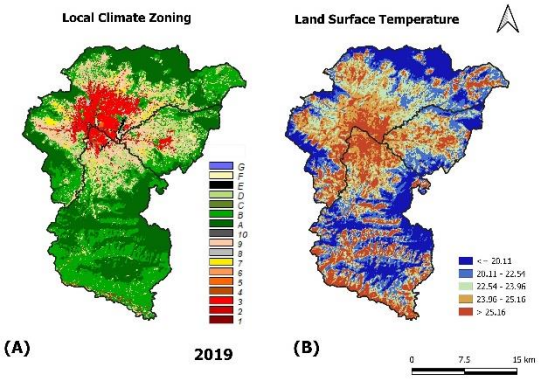

Figure 6: LCZ and LST maps (2013, 2019) of Kathmandu valley

Tribhuvan International Airport, located in Kathmandu has its runway blacktopped because of which the area is categorized as LCZ E (bare rock/ Paved). The outskirts of each city are mostly covered with LCZ D (low Plants); LCZ C (Bush, Scrub); LCG B (Scattered trees), and LCZ A (Dense trees). The core cities of each district are surrounded by LCZ 7(Light Weight low rise). This settlement is an example of sprawl development. The bare Soil (LCZ F) can also be seen in all the cities. The bare soil is due to the extraction of the earth materials by the brick factory and the unmanaged so-called "planned land" with no structures on it.

3.2. Local climate zones and land surface temperature:

Major business areas with compact built-up forms were always warmer compared to their surroundings as seen from Fig.6 and Table 3. Away from the densely built-up areas, the warm parts of the cities also occurred near large patches of relatively flat, impervious surfaces (Road junction, Bus parks, etc.). Hotspots were very often associated with large commercial and distribution areas. On the other hand, bodies of water and forested areas formed the coldest localities.

In general, LST varies significantly across LCZ classes, but the pattern is consistent throughout

cities. The LST of built-up LCZ classes is often greater than that of land cover classes, indicating that urban areas have a high UHI intensity. Among the built-up LCZ classes for Kathmandu Valley, LCZ 3 (compact open-rise) has the highest LST. The LCZ 9 (sparsely built) exhibits the inverse trend. Because most of the LCZ 9 (sparsely developed) areas in Kathmandu and Lalitpur are in steep areas and the villages are bordered by agriculture and forest, the complex and diverse urban morphology of this LCZ class in Kathmandu valley is the primary reason for such an opposing tendency. The urban-rural Ts differences (ΔTs (u–r)) in Kathmandu, Bhaktapur, and Lalitpur that were detected on clear days in the daytime are shown in Fig. 6.

Table 3: LST in different LCZ scheme for both 2019 and 2013 and their differences in (°C)

Building Type	LCZ	LST 2019	LST 2013	LCZ (ºC) (2019-2013)
Compact Midrise	2	25.32	23.99	2
Compact Low-rise	3	27.30	26.694	1
Lightweight Low-rise	7	22.879	21.98	1
Sparsely built	9	23.89	23.66	0
Heavy Industry	10	27.247	23.435	4
Dense Trees	A	17.432	15.78	2
Paved or Bare rock	E	28.789	28.32	0
Bare soil and sand	F	27.60	23.70	4
Water	G	21.25	19.62	1

In general, LST varies significantly across LCZ classes, but the pattern is consistent throughout cities. The LST of built-up LCZ classes is often greater than that of land cover classes, indicating that urban areas have a high UHI intensity. Among the built-up LCZ classes for Kathmandu Valley, LCZ 3 (compact open-rise) has the highest LST. The LCZ 9 (sparsely built) exhibits the inverse trend. Because most of the LCZ 9 (sparsely developed) areas in Kathmandu and Lalitpur are in steep areas and the villages are bordered by agriculture and forest, the complex and diverse urban morphology of this LCZ class in Kathmandu valley is the primary reason for such an opposing tendency. The urban-rural Ts differences (ΔTs (u–r)) in Kathmandu, Bhaktapur, and Lalitpur that were detected on clear days in the daytime are shown in Fig. 6.

Table 4: Comparison of LST with the different LCZ scheme (i.e. LSTLCZX- LSTLCZX) in Kathmandu valley.

Intra building type comparison	Difference in LST (ºC)	Building and Land cover type comparison	Difference in LST (ºC)
LCZ 2-LCZ 7	3	LCZ 2-LCZ A	10
LCZ 3-LCZ 7	4	LCZ 3-LCZ A	11
----------	--	LCZ 7-LCZ A	7

Lower LST is generally observed in land cover LCZ classes due to the extensive previous surface in natural land cover. LCZ A (dense forest) exhibits the lowest LST in the valley. However, because to the seasonal variance in vegetation, there are some anomalies in the LST of land cover groups. In LCZ E (bare rock or paved), higher LST values were reported, with some concrete surfaced sites such as the airport and extensive road networks.

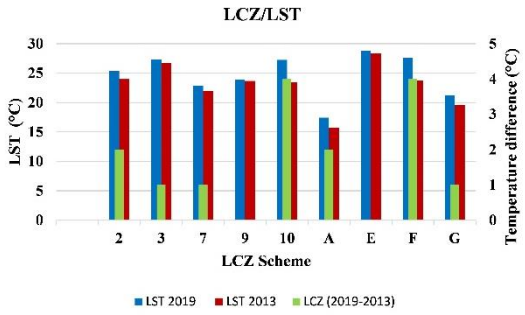

Figure 7: LST vs. LCZ / Difference in LST vs. LCZ (2019-2014)

Within the built-up plan, the difference is roughly 2-4 °C, whereas the difference between Building and Land cover categories is around 5-10 °C (Table 4). As a result, the temperature differential across building and land cover types implies that the UHI effect exists in the Kathmandu valley.

4. Conclusion:

In this study, the surface thermal features of three urban cities were compared, taking into account their specific climatic regions in two different years in same season, month and time. Kathmandu city is very populated and the capital city of Nepal whereas the other two cities are less populated in comparison to Kathmandu. All these

cities are hectically important and the core city is filled with compact settlements.

The comparison was made using clear-sky surface temperature data from Landsat sensors from April 2013 to March 2019. To carry out comprehensive work, LCZ mapping of cities was developed using the widely established WUDAPT methodology, and urban and rural features were demarcated on Landsat 8 according to various LCZ coverage circumstances. The structure of the city, which determines the thermal regimes, can be depicted using LCZ maps. The seasonal changes in LST between urban and rural areas were investigated, and the findings revealed that LCZ division had a significant impact on diurnal LST differences. In the inter-climate comparison, different urban effects were observed – the typical UHI effect was recognized in both 2013 and 2019. The most intense UHI effect was detected in the settlements with compact midrise and compact low-rise, as one might predict. In problem regions, regional plans should focus on lowering built-up area density or providing more open, green places

Additionally, differences were also seen in the intra-climate comparison. The largest difference between the thermal features within the built-up scheme is around 2-4 °C whereas, the comparison between Building and Land cover type is around 5-10 °C (Table 3)

In all cities, increasing the ratio of urban vegetation would be advantageous since I it helps to attenuate urban-induced warming in temperate climates, and (ii) it improves the well-being of residents of cities surrounded by desert, therefore increasing their vegetation cover is advised. To support sustainable local circumstances, the findings of this study should be considered when designing environmental planning and mitigation methods in metropolitan settings.

More detailed remote sensing and surface air temperature datasets are needed to completely understand the link between LST and vegetation. Specifically, soil moisture, in addition to the temporal variation of the vegetation cover, plays an important role in the thermal environment [36]. This variable should be the subject of future investigation. Decision-makers will be able to make more climate-sensitive urban planning decisions if they have a better understanding of the geographical distributions of thermal characteristics and recognize the potentially problematic locations.

Acknowledgements:

We thank the University Grant Commission of Nepal (UGC) for funding and supporting this research, which would not have been feasible otherwise. We'd also want to thank Kantipur City College for supplying us with all of the resources we needed for this study. The University Grant Commission Nepal (UGC) funded this research through Small RDI Grant 2057-76, UGC Award No. SRDI-75/76-Engg-I.

References:

[1] United Nations, “World urbanization prospects: the 2014 revision,” Population Division, Department of Economic and Social Affairs, Now York, 2015.

[2] I. D. Stewart, “Redefining the urban heat island,” T, University of British Columbia, 2011.

[3] Ishtiaque A, Shrestha M, Chhetri N, “Rapid Urban Growth in the Kathmandu Valley, Nepal: "Monitoring Land Use Land Cover Dynamics of a Himalayan City with Landsat Imageries,” Environments, 2017, 4(4):72. https://doi.org/10.3390/environments4040072

[4] Q Weng, “Thermal infrared remote sensing for urban climate and environmental studies: Methods, applications, and trends,” ISPRS Journal of Photogrammetry and Remote Sensing, 2009, 64(4), pp. 335-344.

[5] Sakakibara, Y., Hara, Y., &Kato,Y., “ The feature of heat island intensity with two extra stations method in the southeast part of Koshigaya city, Tenki”, Vol.43, No. 8,pp.537-543,1996.

[6] Mikami, T. “Urban heat island phenomenon and their causing factors: A case study of Tokyo Metropolis”. Journal

of Geography, 114(3), 496-506, 2005. (in Japanese)

[7] Fujimori, Y., Hayashi, Y., & Moriwaki, R. "Characteristic of urban heat island phenomenon in Matsuyama plane". Annual Journal of Hydraulic Engineering,JSCE, 54, 313-318,2010.

[8] Moriwaki, R., Watanabe, K., & Morimoto, K. "Urban Dry Island Phenomenon and its impact on cloud base level". Journal of JSCE,1, 521-529,2013.

[9] Stewart, I.D., & Oke, T. R. "Local Climate Zones for Urban Temperature Studies".Bulletin of the American Meteorological Society, 93, 1879–1900. DOI:10.1175/BAMS-D-11-00019.1,2012.

[10] Bastiaanssena, W.G.M., Menenti, M., Feddes, R.A., & Holtslag, A.A.M. "A remote sensing surface energy balance algorithm for land (SEBAL)". 1. Formulation. Journal of Hydrology,212-213,pg. 198-212, 1998. https://doi.org/10.1016/S0022-1694(98)00253-

[11] Kogan, F.N. "Operational Space Technology for Global Vegetation Assessment". Bulletin of the American Meteorological Society, 82(9), 1949-1964, 2001.

[12] Su, Z. "The surface energy balance system (SEBS) for estimation of turbulent heat fluxes". Hydrology and Earth System Sciences, 6, 85-99,2002.

[13] Arnfield, A.J. " Two decades of urban climate research: a review of turbulence. exchanges of energy and water. and the urban heat island". International Journal of. Climatology, 23(1), 1-26,2003.

[14] Voogt, J., Oke, T. "Thermal remote sensing of urban climate". Remote Sensing Environment,86,370-384,2003.

[15] Weng, Q., &Yang, S. "Managing the adverse thermal effects of urban development in a densely populated Chinese city". Journal of environmental management, 70(2), 145-156,2004. https://doi.org/10.1016/j.jenvman.2003.11.006.

[16] Weng, Q., Hu, X., & Liu, H. "Estimating impervious surfaces using linear spectral". International Journal of Remote Sensing, 30(18), 4807-4830,2009. https://doi.org/10.1080/01431160802665926

[17] Kalma, J.D., McVicar, T.R., & McCabe, M.F. "Estimating Land Surface Evaporation: A Review of Methods Using Remotely Sensed Surface Temperature Data". Surveys in Geophysics, 29, 421-469,2008.

[18] Hansen, J., Ruedy, R., Sato, M., & Lo, R. "Global surface temperature change". Reviews of Geophysics, 48(4),2010. https://doi.org/10.1029/2010RG00034

[19] Vidal, A. "Atmospheric and emissivity correction of land surface temperature measured from satellite using ground measurements or satellite data". International Journal of Remote Sensing, 12(12), 2249-2460,1991. https://doi.org/10.1080/01431169108955279.

[20] Qin, Z., Karnieli, A, & Berliner P. "A mono-window algorithm for retrieving land surface temperature from Landsat TM data and its application to the Israel-Egypt border region". International Journal of Remote Sensing, 22(18),3719-3746,2001. https://doi.org/10.1080/01431160010006971.

[21] Jiménez-Muñoz, J.C., Sobrino J.A. "A generalized single-channel method for retrieving land surface temperature from remote sensing data". Journal of Geophysics Research, 108(D22), 4688,2003. https://doi.org/10.1029/2003JD003480.

[22] UNISDR "Making Development Sustainable: The Future of Disaster Risk Management. Global Assessment Report on Disaster Risk Reduction". Geneva, Switzerland: United Nations Office for

Disaster Risk Reduction (UNISDR).2015.

[23] Thapa, R.B.., Murayama, Y. "Scenario-based urban growth allocation in Kathmandu Valley, Nepal". Landscape and Urban Planning, 105(1-2), 140-148,2012.

[24] Thapa R. B., Murayama Y. and Ale S. "Kathmandu". Cities, 25, 45-57,2008.

[25] Lelovics, E., Unger, J., Gál, T., and Gál, C. V. "Design of an urban monitoring network based on Local Climate Zone mapping and temperature pattern modeling". Climate Research, 60,51–62,2014. Doi: 10.3354/cr01220, 2014.

[26] Gamba, P., Lisini, G., Liu, P.,Du P. and Lin,H. "Urban climate zone detection and discrimination using object-based analysis of VHR scenes". Proc. 4th GEOBIA, 7–9,2012.

[27] Weng, Q. "Global Urban Monitoring and Assessment through Earth Observation". CRC Press,pp. 420,2014.

[28] Bachtel, B., Alexander, P.J., Böhner, J., Ching, J., Conrad, O., Feddema, J., Mills, G., See, L., & Stewart, I.D."Mapping Local Climate Zones for a Worldwide Database of the Form and Function of Cities", ISPRS International Journal of Geo-Information, 199-219,2015. Doi:10.3390/ijgi4010199

[29] Bechtel, B., & Daneke, C. "Classification of Local Climate Zones Based on Multiple Earth Observatory Data". IEEE J. Sel. Top. Appl. Earth Obs. Remote Sensing, 5, 1191-1202,2012.

[30] Thapa Chhetri, D.B., Fujimori, Y., & Moriwaki, R. "local climate classification and urban heat/dry island in Matsuyama plain". Journal of Japan Society of Civil Engineers Ser B1(Hydraulic Engineering), 73(4) , 487-492,2017.

[31] Kaplan, G., Avdan, U. and Avdan, Z. Y. "Urban heat island analysis using the Landsat 8 satellite data: A case study in Skopje, Macedonia", Multidisciplinary Digital Publishing Institute Proceedings, Vol. 2, p. 358,2018.

[32] Weng, Q., Lu, D., & Schubring, J. "Estimation of land surface temperature-vegetation abundance relationship of urban heat island studies". Remote Sensing of Environment, 89(4), 467-483,2004. https://doi.org/10.1016/j.rse.2003.11.005.

[33] Landsat Project Science Office. "Landsat 7 Science Data User's Handbook. NASA's Goddard Space Flight Center",Greenbelt,186,2002. http://landsathandbook.gsfc.nasa.gov/pdfs/Landsat7_Handbook.pdf

[34] Sobrino, J.A., Jiménez-Muñoz, J.C., & Paolini, L. "Land surface temperature retrieval from Landsat TM 5". Remote Sensing Environment, 90,434–440,2004.

[35] Carlson, T.N., & Ripley, D.A. "On the relation between NDVI, fractional vegetation cover, and leaf area index". Remote Sensing Environment. 62, 241–252,1997.

[36] Seneviratne, S. I., Lüthi, D., Litschi, M., & Schär, S. "Land–atmosphere coupling and climate change in Europe". Nature, 443, 205-209,2006. Doi:10.1038/nature05095

[37] A. L. Sorrel, "Professionalism in action," Tex. Med., vol. 111, no. 3, pp. 51–57, 2015.

ACRONYMS

C	Celsius
CDAS	Command and Data Acquisition Station
DEM	Digital Elevation Model
EOS	Earth Observation Satellite
ETM+	Enhanced Thematic Mapper Plus
F	Fahrenheit
GIS	Geographic Information System
GSICS	Global Space-based Inter Calibration System
K	Kelvin
KV	Kathmandu Valley
LCZ	Local Climate Zones
LDCM	Landsat Data Continuity Mission
LIDAR	Light Detection and Ranging
LST	Land Surface Temperature
LULC	Land Use and Land Cover
MSS	Multispectral Scanner System
NIR	Near Infrared

OLI	Operational Land Imager
ROI	Region of Interest
RS	Roughness sub-layer
SAGA GIS	System for Automated Geoscientific Analyses
SRTM	Shuttle Radar Topography Mission
SW	Short Wave
SWIR	Shortwave Infrared
TIR	Thermal Infrared
TIRS	Thermal Infrared Sensor
TM	Thematic Mapper
TOA	Top of the Atmosphere
UBL	Urban Boundary Layer
UDI	Urban Dry Island
UHI	Urban Heat Island
USGS	United States Geological Survey
WUDAPT	World Urban Database and Access Portal Tool